SIRM 2015 – 11th International Conference on Vibrations in Rotating Machines,
Magdeburg, Deutschland, 23. – 25. February 2015

Turbocharger rotors with oil-film bearings: sensitivity and optimization analysis in virtual prototyping

P. Koutsovasilis [1], **N. Driot** [2]

[1,2] Rotordynamics & Preventive Acoustics, Global Engineering Core Science, BorgWarner Turbo Systems Engineering GmbH, DE-67292 Kirchheimbolanden, {pkoutsovasilis, ndriot}@borgwarner.com

Abstract

The correct capture and understanding of the bearing induced rotor vibrations is nowadays a rather compulsory task, which should accompany the modeling and simulation work flow of high-speed rotor systems, such as turbochargers. The oil-film concentrated in the rotor's journal bearings is the root cause of the systems occurring non-linear effects known as sub-synchronous vibrations. In this paper the virtual prototype process of turbocharger rotors with full-floating bearings is presented, which is conducted based on data mining, sensitivity analysis and non-supervised neural network methods for three levels of the system's assembly: the wheel-shaft-bearing center of masses distribution, the bearing-shaft geometry and the wheel unbalance levels. The impact of each design parameter on the system's stability is verified by quantifying their influence upon the sub-synchronous evolution and the inner and outer oil-film load capacity. On this account design configurations are indicated that could be set as a compromise in terms of feasibility and low-cost production.

1 Introduction

The turbocharger rotor-bearing model with oil-film ring bearings is defined as an assembly of rigid and flexible bodies, which interact with each other due to the presence of joints and force elements (Fig. 1). The motion equations of such constrained mechanical multi body systems [26, 27] are given by second order, index-3 Differential-Algebraic Equations (DAE) [2, 1, 4, 8]:

$$\mathbf{M}(\mathbf{q})\ddot{\mathbf{q}}(t) = \mathbf{h}(\mathbf{q}, \dot{\mathbf{q}}, t) - \mathbf{G}^T(\mathbf{q}, t)\boldsymbol{\lambda} \tag{1}$$

$$\mathbf{0} = \mathbf{g}(\mathbf{q}, t). \tag{2}$$

Here, $\mathbf{q}^T \in \mathbb{R}^{n\times 1}, n \in \mathbb{N}^*$ represents the set of generalized coordinates, $\mathbf{M} \in \mathbb{R}^{n\times n}$ the symmetric mass matrix and $\mathbf{h}(\mathbf{q}, \dot{\mathbf{q}}, t) \in \mathbb{R}^{n\times 1}$ the vector containing all applied and velocity dependent inertia forces. The generalized constraint forces $-\mathbf{G}^T(\mathbf{q}, t)\boldsymbol{\lambda} \in \mathbb{R}^{n\times 1}$ are defined by the associated Jacobian matrix $\mathbf{G} := (\partial \mathbf{g}/\partial \mathbf{q})(\mathbf{q}, t)$ and the Lagrange multipliers $\boldsymbol{\lambda} \in \mathbb{R}^{n_c}$ satisfying the existing n_c constraints. While the wheels and journal bearings are modeled as rigid bodies including the associated unbalance effects (Fig. 1), the shaft is introduced as a flexible body, which is FE-discretized and incorporated in (1)-(2) as a Component-Mode-Synthesis reduced order model [7, 6, 15, 16, 17, 3].

The root cause of the sub-synchronous vibrations -also known as oil-whirl/whip- is the oil-film concentrated in the rotor journal bearings, which in case of turbocharger rotors with full-floating ring bearings drives the system to exhibit the following basic sub-synchronous responses [3, 22, 24, 5, 9, 29, 25]:

1. 1st sub-synchronous (Sub_1) with the oil whirl/whip of the inner oil film exciting the gyroscopic conical forward mode,
2. 2nd sub-synchronous (Sub_2) with the oil whirl/whip of the inner oil film exciting the gyroscopic cylindrical forward mode,
3. 3rd sub-synchronous (Sub_3) with the oil whirl/whip of the outer oil film exciting the gyroscopic conical forward mode.

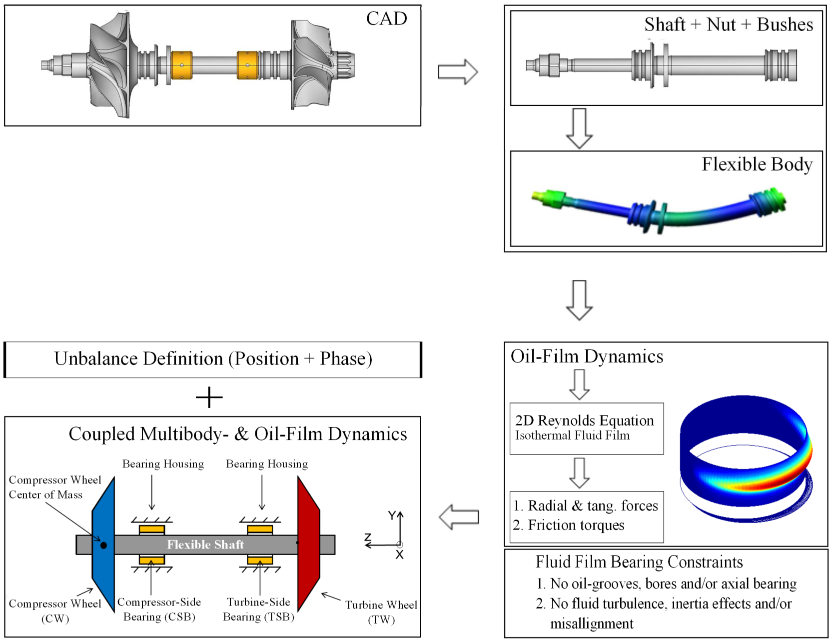

Figure 1: Turbocharher rotordynamics - modeling procedure

The aforementioned oil-whirl/whip effects are captured by solving the Reynolds equation [28, 5, 3, 24] for both the inner and outer film, which in the framework of the current work undergo the restrictions quoted in Fig. 1. The calculated fluid film forces along with the friction torques are incorporated into (1)-(2) for conducting the rotor dynamic simulations. The rotor is driven by a prescribed motion applied at the turbine wheel center of mass (Fig. 1).

The turbocharger run-up virtual prototype process presented within the framework of this paper is applied for three levels of the system's assembly: the wheel-shaft-bearing center of masses design, the bearing-shaft geometry and the wheel unbalance levels. Each assembly level undergoes separately a variation study with which design parameters are identified and assessed according to their impact on the sub-synchronous evolution and the inner and outer oil-film load capacity. All above is conducted for an example rotor system with its' basic configuration

Table 1: Virtual prototype process - basic rotor assembly information

Design information of rotor assembly	Approximate value($\approx$)	Unit
Total rotor assembly mass	70	[g]
Total rotor assembly length	100	[mm]
Bearing ring inner & outer diameter	6 & 9.5	[mm]
Bearing ring inner & outer width	3.5 & 6	[mm]
Reference bearing shaft diameter D	6	[mm]
Dynamic oil viscosity at $20°C$	0.16	[Ns/m^2]

being given in Table 1. It copes with a small-sized high-speed turbocharger rotor with full-floating ring bearings, which operates under high oil-supply temperatures (150°C). The size as well as the maximum operating speed ($3 \cdot 10^5$ RPM) indicates for the aforementioned vibration effects (Sub$_2$ & Sub$_3$) not to be avoidable. While Sub$_2$ could be listed under comfort-issue problems, Sub$_3$ with extended amplitudes might lead to rotor destruction.

It should be mentioned that the results presented in this paper are valid only for the investigated turbocharger rotor, i. e. generalizations are not advisable.

2 Turbocharger run-up virtual prototype process

2.1 First assembly level: wheel-shaft-bearing center of mass design

The first assembly level considers the system's basic design geometry based on center of mass distribution of all the system's rigid bodies as given in Fig. 2. The distance between the center of masses L_{CB} (compressor wheel

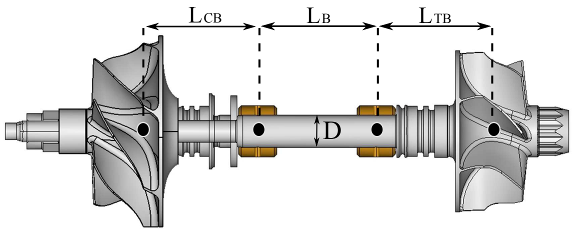

Figure 2: First assembly level [18]

to compressor side bearing), L_B (compressor side to turbine side bearing) and L_{TB} (turbine side bearing to turbine wheel) depicted in Fig. 2 are set as independent parameters for a variation study, which is defined in terms of a Design of Experiment (DoE) [20]. Additionally, the diameter D of the shaft-part located between the two bearings (Fig. 2) is set as an extra DoE-parameter. Herewith, various rotor assemblies are generated, all of which have both different shaft diameter and total length. This implies that the flexible shaft modeling process described in Section 1 and Fig. 1 should be repeated according to the associated dimension of the DoE (in this case 20 configurations were computed).

It is worth mentioning that the methodology applied is not restricted on how to vary the investigated parameters. Here, it is conducted by means of a DoE, but the application of multivariate analysis algorithms for defining the parameter space with the help of sampling methods, e.g. random, Monte Carlo, Latin Hypercube, etc., is not excluded [11, 19].

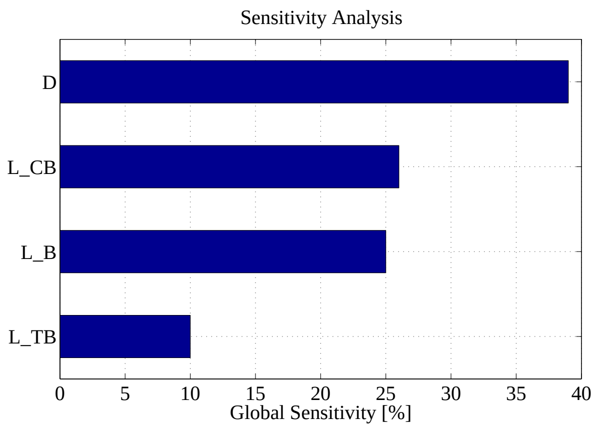

Figure 3: First assembly level - Sensitivity analysis [18]

The importance of each parameter upon the global set of responses, i. e. sub-synchronous vibrations and inner/outer oil-film capacity, is assessed by applying the sensitivity analysis algorithm (Appendix A.1). The shaft diameter D is quantified as being the most influential input variable (39%). On the other hand, the role of L_{TB} is subordinate (10%), whereas L_{CB} and L_B are rated as equally important (26% and 25%, respectively).

Amongst other methods, response surface methodology [21, 20, 12, 23] delivers an insight on the positive or negative influence of each parameter on the designated response space. In this regard Fig. 4 combined with the global sensitivity information reveals the possibilities of improved designs with respect to Sub_1, Sub_2 and Sub_3, but also depict the controversial effect a single parameter can have on several sub-synchronous responses (e.g. a large shaft diameter affects positively the Sub_1-, but negatively the associated Sub_2-amplitude, etc.). This means the best suitable compromise should be found, which in case of the examined rotor would be a decrease of D and L_{CB} and an increase of L_B. L_{TB} has a minor impact on the system's responses (Fig. 3), therefore it should remain unchanged.

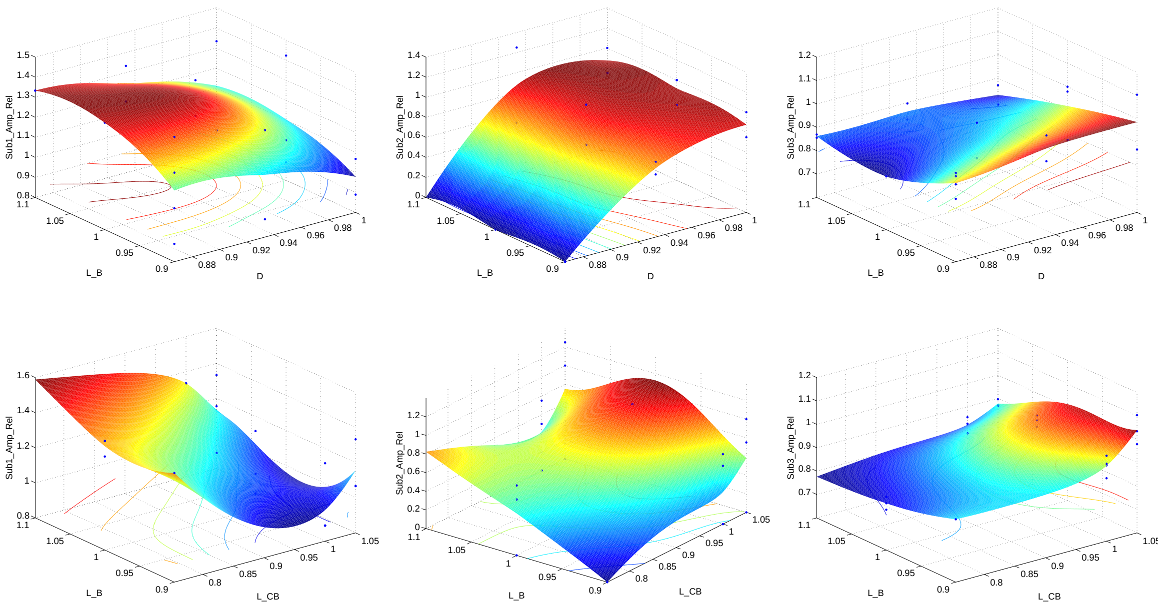

Figure 4: First assembly level - Response surface methodology for the $\text{Sub}_{1,2,3}$ relative amplitudes - Normalized Data [18]

2.2 Second assembly level: shaft-bearing dimension design

The second assembly level copes with the detailed information with respect to the shaft and bearing design [18], which is directly set as an input for the Reynolds equation of lubrication in the inner and outer oil-film bearing [28, 5, 3, 24] under the restrictions quoted in Fig. 1. On this account, the parameters selected for this specific DoE study of 45 configurations are given in Table 2. Both the inner and outer bearing diameter are primarily not introduced as design parameters due to often occurring packaging restrictions, although their correlation with hydrodynamic friction [19], bearing speed ratio and thus, Sub_3 minimization is well known.

Table 2: Assembly level two: shaft-bearing dimension design

Parameter	Description
D_1 and D_2	CSB and TSB shaft diameter
CSB_{ψ_i} and CSB_{ψ_o} & CSB_{W_i}, CSB_{W_o}	CSB inner and outer clearance & CSB inner and outer width
TSB_{ψ_i} and TSB_{ψ_o} & TSB_{W_i}, TSB_{W_o}	TSB inner and outer clearance & TSB inner and outer width
T_{sup}	Oil-supply temperature with $T_{sup}^{min} = 90°C$ & $T_{sup}^{max} = 150$°C
CSB: Compressor-Side-Bearing & TSB: Turbine-Side-Bearing	

The sensitivity analysis results for the second assembly level are depicted in Fig. 5. Almost 40% of the system's response is controlled by the design of the outer clearances (CSB_{ψ_o} & TSB_{ψ_o}). The application of smaller outer clearances for Sub_3 vibrations is an experience-based solution, which in the framework of the current analysis is in addition quantified.

The bearings' outer width is further listed as important factors, which along with the outer clearances contribute in influencing over 55% of the system's response. An enlargement of the bearing outer width although Sub_3-beneficial, it acts contra-productive w.r.t. to constant tone problems (Sub_2) as seen in Fig. 6. The oil-supply

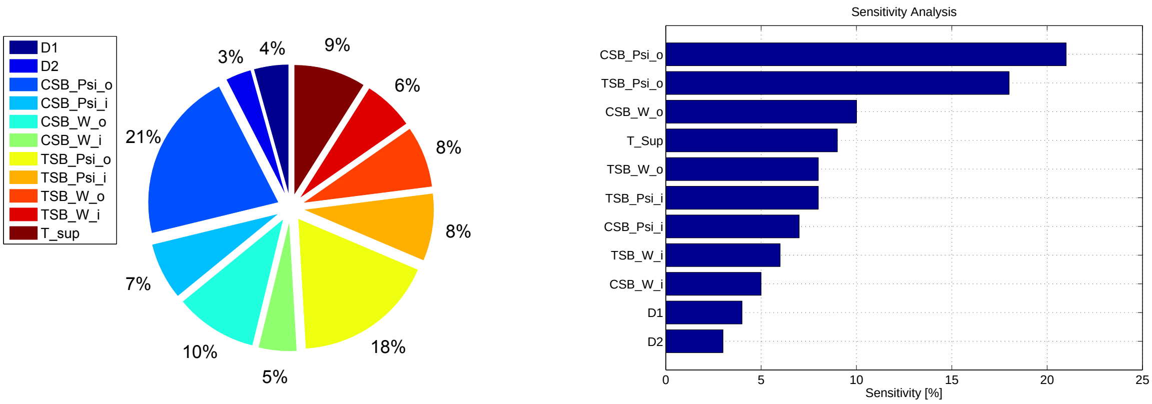

Figure 5: Second assembly level - Sensitivity analysis [18]

temperature T_{sup} is ranked as the fourth most important parameter. Since, a turbocharger rotor has to perform equally well under cold and warm conditions, the presented results are extended by applying the Self Organizing Maps (SOM) methodology [13, 14, 18] (Appendix A.2) in order to account for feasible rotor-assembly designs that would hold on to the temperature prerequisites. On this account a Sub_3 best case scenario (elliptical selected cells in Fig. 6) and a compromise $Sub_{1,2,3}$ scenario (rectangular selected cells in Fig. 6) is proposed.

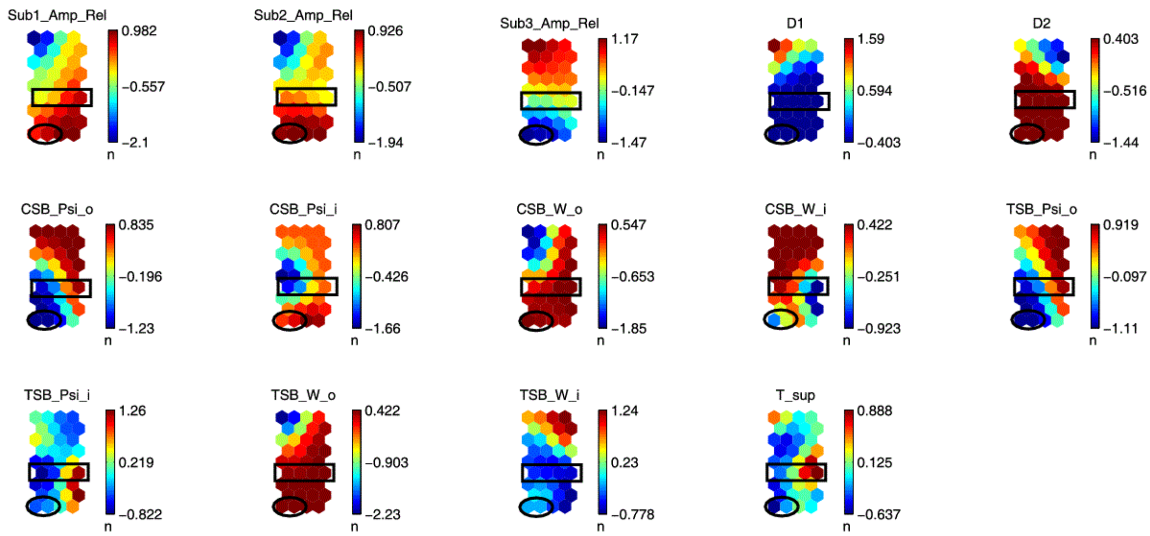

Figure 6: SOM analysis: Sub_3 best case scenario (elliptical selected cells) & compromise $Sub_{1,2,3}$ scenario (rectangular selected cells) - Normalized responses [18]

Table 3: Assembly level two - Improved design based on the reference configuration of Table 1 [18]

Parameter \ Assembly level two	Best Sub_3 configuration	Compromise $Sub_{1,2,3}$ configuration
D_1 & D_2	$\searrow$ & $=$	$\searrow$ & $=$
CSB_{ψ_o} & TSB_{ψ_o}	$\searrow$ & $\searrow$	$=$ & $=$
CSB_{ψ_i} & TSB_{ψ_i}	$=$ & $=$	$=$ & $\nearrow$
CSB_{W_o} & TSB_{W_o}	$\nearrow$ & $\nearrow$	$\nearrow$ & $\nearrow$
CSB_{W_i} & TSB_{W_i}	$=$ & $\searrow$	$\searrow$ & $\searrow$

"$\searrow$", "$\nearrow$" and "$=$" indicate parameters with dimension smaller, larger and equal than the associated parameter of the reference configuration rotor-assembly, respectively

2.3 Third assembly level: wheel unbalance dimension design

The third and final assembly level takes into consideration the unbalance information introduced into the system (Fig. 1) after having completed the previous two assembly level steps. Herewith, the recommended bearing design undergoes a robustness test coping for the uncertain real-life unbalance configurations. It is conducted by accounting for several feasible unbalance magnitude and phase configurations for the four unbalance planes (left-hand side of Fig 7).

Apart form the standardized force and rotor coupling configurations, the rest of $0°$ and $180°$ phase configurations per unbalance plane are tested for sub-synchronous robustness. It an important task, since the rotor-bearing systems behaves highly non linear under different unbalance phase configurations. On this account, it is shown (Fig. 7) that the first and last unbalance levels result in having the greatest sensitivity with respect to the harmful Sub_3 response, i.e. Sub_3-magnitude and duration, respectively.

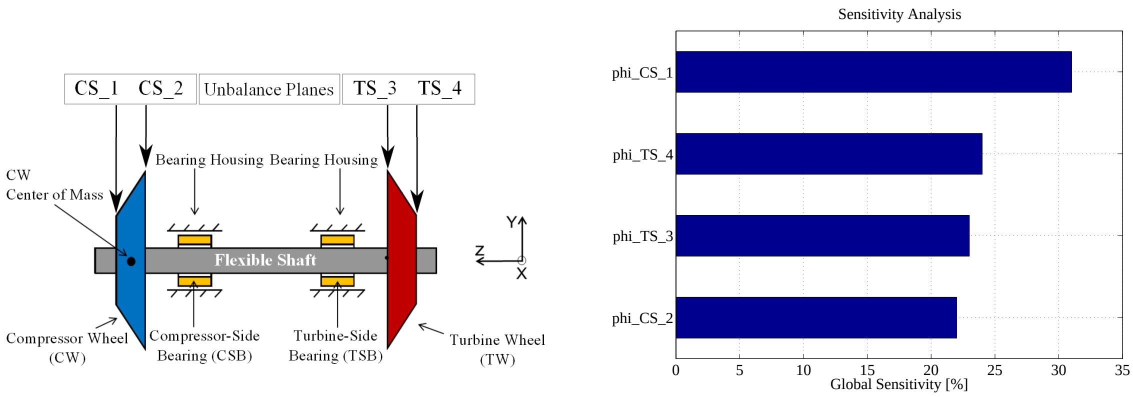

Figure 7: Left: unbalance planes - Right: sensitivity analysis for the unbalance phase of each plane upon the Sub_3 evolution, i.e. Sub_3-magnitude and -duration

On the basis of the aforementioned, the three level assembly process along with the noted bearing diameter effects [19] leads to the generation of a compromise model, which compared to the reference configuration shows better controlled sub-synchronous responses (Fig. 8). The comparison is conducted by means of the radial displacement of the compressor's wheel center of mass (Fig. 1, 7) as well as the frequency decomposition of this signal.

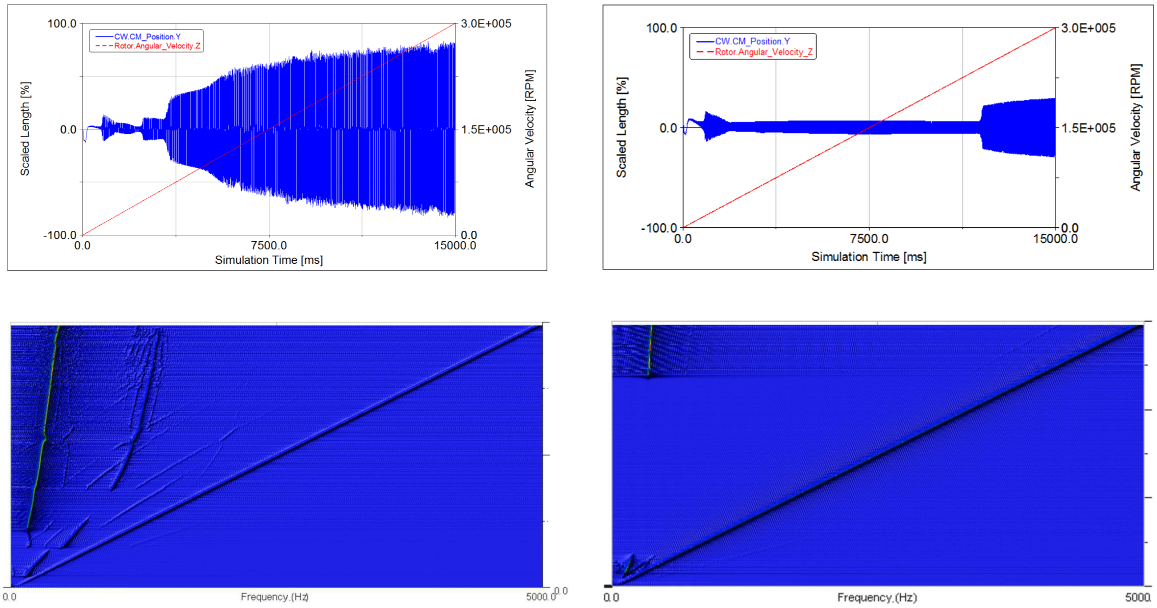

Figure 8: Left: reference - Right: DoE result - Comparison of the compressor wheel's center of mass radial displacement & waterfall diagram

3 Conclusion

In this paper the virtual prototype process of turbocharger rotors with full-floating bearings is presented, which is conducted based on data mining, sensitivity analysis and non-supervised neural network methods for three levels of the systems assembly: the wheel-shaft-bearing center of masses distribution, the bearing-shaft geometry and the wheel unbalance levels. The impact of each design parameter on the systems stability is verified by quantifying their influence upon the sub-synchronous evolution. Additionally, the recommended bearing design undergoes a robustness test coping for the uncertain real-life unbalance configurations. It is conducted by accounting for several feasible unbalance magnitude and phase configurations for the four unbalance plane and the inner and outer oil-film load capacity. On this account design configurations are indicated that could be set as a compromise in terms of feasibility and low-cost production.

REFERENCES

[1] Arnold, M., Burgermeister, B., Führer, C., Hippmann, G., Rill, G. Numerical methods in vehicle system dynamics: State of the art and current developments. *Vehicle System Dynamics*, 49:1159–1207, 2011.

[2] Arnold, M., Burgermeister, B., Führer, C., Hippmann, G., Rill, G. Simulation algorithms and software tools. In *G. Mastinu, M. Plöchl (eds.): Road and Off-Road Vehicle System Dynamics Handbook*, pages 45–68. 2014.

[3] Boyaci, A., Backhaus, K., Koch, R. Hochlaufsimulation: Mehrkörpersimulation des Hochlaufverhaltens von ATL-Rotoren mit nichtlinear modellierten Schwimmbuchsenlagern. Technical Report 889, FVV e. V., 2009.

[4] Brenan, K. E., Campbell, S. L., Petzold, L. R. *Numerical solution of initial-value problems in differential-algebraic equations*. Classics in Applied Mathematics. SIAM - Society for Industrial and Applied Mathematics, 1996.

[5] Butenschön, H.J. *Das hydrodynamische, zylindrische Gleitlager endlicher Breite unter instationärer Belastungen*. PhD thesis, TH Karlsruhe, 1976.

[6] Craig, Jr. R. R. Coupling of substructures for dynamic analyses: an overview. *AIAA-2000-1573*, 2000.

[7] Craig, R., Bampton, M. Coupling of substructures in dynamic analysis. *AIAA*, 6, 1968.

[8] García de Jalón, J., Gutiérrez-López, M. D. Multibody dynamics with redundant constraints and singular mass matrix: existence, uniqueness, and determination of solutions for accelerations and constraint forces. *Multibody System Dynamics*, 30:311–341, 2013.

[9] Gasch, R., Nordmann, R., Pfützner, H. . *Rotordynamik*. Springer, 2. edition, 2001.

[10] Golub, G. H., Van Loan, C. F. *Matrix computations*. The John Hopkins University Press, 1996.

[11] Hammersley, J. M., Handscomb, D. C. *Monte Carlo methods*. Fletcher, 1975.

[12] Jobson, J. D. *Applied multivariate data analysis: regression and experimental design*. Springer Verlag, 4. edition, 1999.

[13] Kohonen, T. The self-organizing map. In *Proc. IEEE*, volume 78, pages 1464–1480, 1990.

[14] Kohonen, T. *Self-organizing maps*, volume 30 of *Information Sciences*. Springer-Verlag, 2. edition, 1997.

[15] Koutsovasilis, P. *Model order reduction in structural mechanics: coupling the rigid and elastic multi body dynamics*. PhD thesis, Technische Universität Dresden, 2009.

[16] Koutsovasilis, P. Improved component mode synthesis and variants. *Multibody System Dynamics*, 29:343–359, 2013.

[17] Koutsovasilis, P., Beitelschmidt, M. Model order reduction of finite element models: improved component mode synthesis. *Mathematical and Computer Modelling of Dynamical Systems*, 16(1):57–73, 2010.

[18] Koutsovasilis, P., Driot, N., Lu, D., Schweizer, B. Quantification of sub-synchronous vibrations for turbocharger rotors with full-floating ring bearings *(accepted)*. *Archive of Applied Mechanics*, 2014.

[19] Koutsovasilis, P., Schweizer, B. Parameter variation and data mining of oil film bearings - a stochastic study on the Reynolds equation of lubrication. *Archive of Applied Mechanics*, 80(9):1017–43, 2014.

[20] Montgomery, D. C. *Design and analysis of experiments*. John Wiley & Sons, 6. edition, 2005.

[21] Montgomery, D. C., Myers, R. H. *Response surface methodology: process and product in optimization using designed experiments*. John Wiley & Sons, 1995.

[22] Nguyen-Schäfer, H. *Rotordynamics of automotive turbochargers: linear and nonlinear rotordynamics - bearing design - rotor balancing*. Springer-Verlag Berlin Heidelberg, 2012.

[23] Sathyanarayana, K. K. MATLAB GUI Implementierung - Statistik & Data Mining. Studienarbeit, Institut für Wissenschaftliches Rechnen, Technische Universität Braunschweig, 2013.

[24] Schweizer, B. Vibrations and bifurcations of turbocharger rotors. In *SIRM 2009 - 8th International Conference on Vibrations in Rotating Machines*, 2009.

[25] Schweizer, B., Sievert, M. Nonlinear oscillations of automotive turbocharger turbines. *Journal of Sound and Vibration*, 321:955975, 2009.

[26] Schwertassek, R., Wallrapp, O. *Dynamik flexibler Mehrkörpersysteme: Methoden der Mechanik zum rechnergestützten Entwurf und zur Analyse mechatronischer Systeme*. Vieweg, 1999.

[27] Shabana, A. A. *Dynamics of multibody systems*. Cambridge University Press, University of Illinois at Chicago, 2005.

[28] Szeri, A. Z. *Fluid film lubrication: theory and design*. Cambridge University Press, 2005.

[29] Vance, J. M. *Rotordynamics of turbomachinery*. John Wiley and Sons, 1988.

[30] Vesanto, J., Alhoniemi, E., Himberg, J., Kiviluoto, K., Parhankangas, J. Self-organizing map for data mining in MATLAB: the SOM toolbox. *Simulation News Europe*, 25(54), 1999.

A Appendix

A.1 Appendix: Sensitivity analysis

The application of Redundancy Analysis (RDA) [10, 12, 23, 18] contributes in locating certain sensitivity origins among the variables and responses. Aim is to locate the most influencing variables with respect to not only one selected response, but either all or a set of responses.

Linear regression analysis is performed on the matrix of the responses $\mathbf{R}$ using the matrix of variables $\mathbf{V}$ and then a standard Principal Component Analysis (PCA) is conducted on the approximate matrix obtained by multidimensional regression [10]. The set of responses $\mathbf{R}$ is varied according to the set of variables $\mathbf{V}$ and thus, the multi linear regression model can be formulated for each response $\mathbf{R}_i$ individually (3)-(4), i.e.

$$\underbrace{\begin{bmatrix} r_1 \\ r_2 \\ \vdots \\ r_p \end{bmatrix}}_{\mathbf{R}_i} = \underbrace{\begin{bmatrix} 1 & v_{11} & v_{12} & \cdots & v_{1m} \\ 1 & v_{21} & v_{22} & \cdots & v_{2m} \\ \vdots & \vdots & \vdots & \ddots & \vdots \\ 1 & v_{p1} & v_{p2} & \cdots & v_{pm} \end{bmatrix}}_{\mathbf{V}} \underbrace{\begin{bmatrix} b_0 \\ b_1 \\ \vdots \\ b_m \end{bmatrix}}_{\mathbf{b}_i} + \underbrace{\begin{bmatrix} \epsilon_1 \\ \epsilon_2 \\ \vdots \\ \epsilon_n \end{bmatrix}}_{\boldsymbol{\epsilon}_i}, \quad i = 1, 2, \cdots, n \tag{3}$$

$$\mathbf{B} = [\mathbf{b}_1 \ \mathbf{b}_2 \ \cdots \ \mathbf{b}_i] \in \mathbb{R}^{m \times n} \quad \text{where} \quad \mathbf{b}_i = (\mathbf{V}^\mathbf{T}\mathbf{V})^{-1}\mathbf{V}^\mathbf{T}\mathbf{R}_i \tag{4}$$

The vector $\mathbf{G}$ containing the sensitivity coefficients is formulated by calculating the euclidean norm for each of the row vectors of the regression coefficient matrix $\mathbf{B}$, i.e.

$$\mathbf{G} = \left[\ \left\|\tilde{\mathbf{b}}_1\right\| \ \left\|\tilde{\mathbf{b}}_2\right\| \ \cdots \left\|\tilde{\mathbf{b}}_j\right\| \ \right]^T \in \mathbb{R}^{m \times 1} \quad \text{with } \tilde{\mathbf{b}}_j, j = 1, \cdots, m \text{ being the row vector of } \mathbf{B} \text{ in (4).} \tag{5}$$

A.2 Appendix: Self Organizing Map (SOM)

The Self Organizing Map (SOM) methodology is applied [13, 14] using the SOM Matlab toolbox [30]. For the purpose of the current study the sequential training algorithm has been applied, which is briefly outlined in the following based on the exact description given in [19, 18]. For an in-depth description of the method see [30, 13, 14].

Assume the high dimensional input data (variables and responses in Section 3) be represented by a d-dimensional set of vectors. A weight vector $M = [m_1 \ \ m_2 \ \ ... \ \ m_d]^T \in \mathbb{R}^d$ is associated with each element of the SOM array, which additionally is of equal dimension. At each training step, a random sample vector $\mathbf{x}$ is selected from the input set and the associated distances w.r.t. to the weight vectors are calculated. Herewith, the Best Matching Unit (BMU) is ascertained [13], which is calculated by allocating the node index c with the minimum distance -Euclidean distance- from the input vector [30]:

$$\|\mathbf{x} - \mathbf{m}_c\| = \min_i \{\|\mathbf{x} - \mathbf{m}_i\|\} \tag{6}$$

The SOM weight vectors $\mathbf{m}_i$ are updated such that BMU gradually approaches the input vector in the input space with the associated BMU topological neighbors conducting the same procedure. The time dependent update algorithm used therefore is [30, 13, 14]:

$$\mathbf{m}_i(t+1) = \mathbf{m}_i(t) + \alpha(t)h_{ci}(t)\left[\mathbf{x}(t) - \mathbf{m}_i(t)\right], \tag{7}$$

with $\alpha(t)$ being the monotonically decreasing learning rate [30, 13, 14], $h_{ci}(t)$ the neiborhood function around the computed unit c and t the time. A random initialization scheme is chosen for the SOM generation and the Gaussian function is used for allocating the neighborhood function $h_{ci}(t)$ as defined in [30], i.e.

$$h_{ci}(t) = e^{-d_{ci}^2/2\sigma_t^2} \tag{8}$$

σ_t : neighborhood radius at time t

d_{ci} : distance between the map units c and i on the map grid